Catalysis Letters (2022) 152:689–698
https://doi.org/10.1007/s10562-021-03668-8

Biomimetic Mineralization of Prussian Blue Analogue-Incorporated Glucose Oxidase Hybrid Catalyst for Glucose Detection

Bin Chen[1] · Xiaoling Wu[1] · Jun Xiong[1] · Min-Hua Zong[1] · Jian-Hua Cheng[2] · Jun Ge[3] · Wen-Yong Lou[1,2]

Received: 4 March 2021 / Accepted: 16 May 2021 / Published online: 22 May 2021

Abstract

A copper analogue of Prussian blue incorporated multienzyme system was successfully established via a biomimetic mineralization process, whereas CPB with peroxidase-like activity provided protecting effect for encapsulated glucose oxidase from attack in hostile conditions. The hybrid composite was developed as a colorimetric biosensor for ultrasensitive detection of glucose, with a low detection limit (0.48 μM).

Graphic Abstract

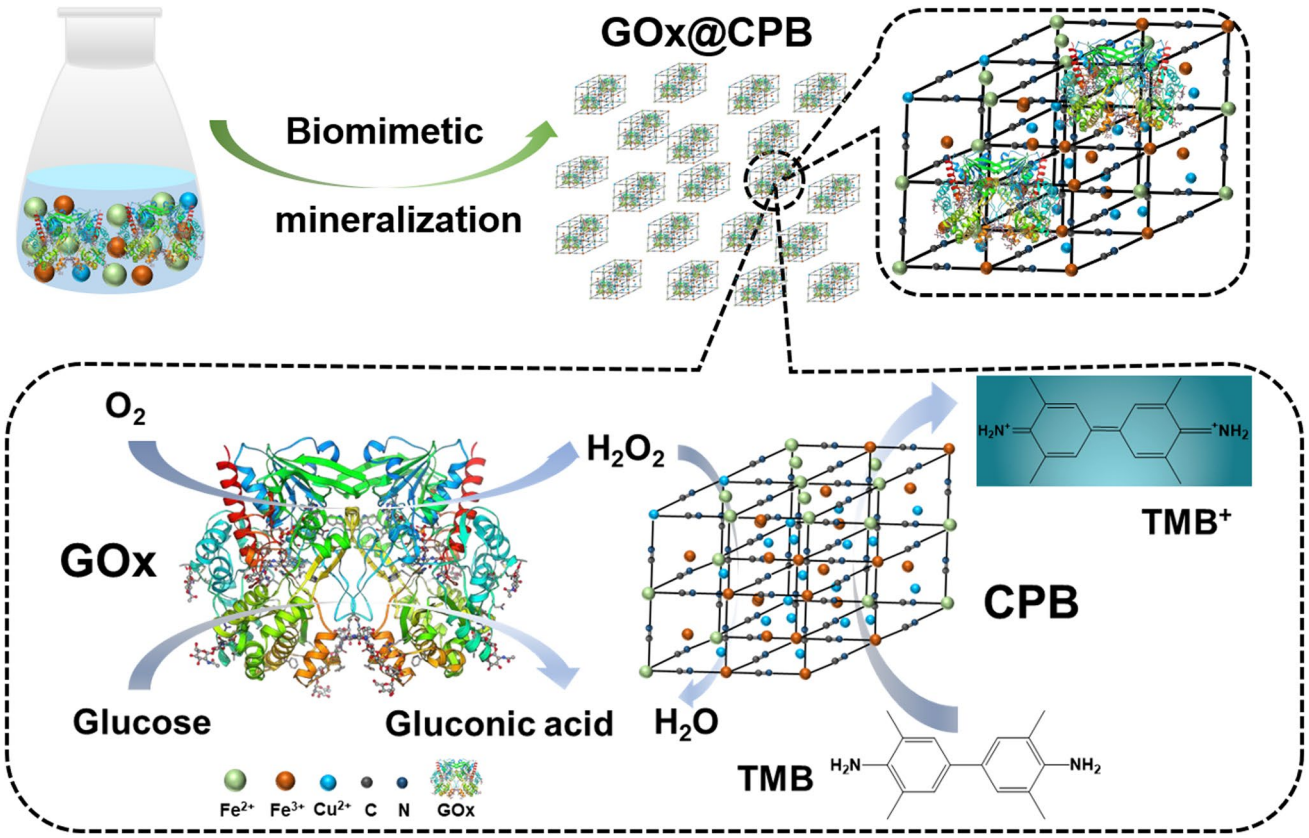

Keywords Prussian blue analogue · Biomimetic mineralization · Hybrid catalyst · Cascade reaction · Glucose detection

Extended author information available on the last page of the article

1 Introduction

Biological processes such as energy conversion, biosynthesis, and detoxification occurring inside cells usually involve cascade reactions, driven by the cooperation of multiple enzymes located in compartments of subcellular organelles [1]. The confined space enables the entrapment and accumulation of intermediates and minimizes their diffusion into the bulk solution, leading to an enhanced catalytic efficiency of the multienzyme system [2]. Thus, the in vitro synthesis of artificial multienzyme systems to mimic the cascade reactions taking place in cells holds great promise in the fields of biocatalysis [3, 4], biosensing [5], pharmaceuticals [6], and others [7, 8]. Considerable efforts have been made to develop multienzyme systems by combining different enzymes, for example, using DNA or protein scaffolds as bridges [9, 10]. However, the low operational stability, sensitivity to environmental stress, and difficult recycling of the enzyme have hindered the wide application of this approach. Therefore, the development of efficient strategies for the construction of highly active and robust multienzyme catalytic systems is needed [11, 12].

Biomimetic mineralization [13–17] is a recently developed facile strategy for enzyme encapsulation, in which biomacromolecules including proteins or nucleic acids participate in and regulate the crystallization and formation of inorganic materials, leading to the successful encapsulation of target biomolecules inside them. The formed inorganic material serves as a protecting shell for the encapsulated biomacromolecules and shields them from the attack of heat, organic solvents, and protease from working conditions [18]. For example, metal–organic frameworks (MOFs) have been employed for the encapsulation of a large number of enzymes [19–21], antibodies [22], DNA [23], and even cells [24]. The MOFs enabled the encapsulated species to function under unfavorable conditions and thus received considerable attention. Taking advantage of the catalytic activity of the supporting inorganic material is expected to endow the encapsulated species with additional functionalities and enable new applications. However, this aspect has not been fully investigated.

Prussian blue (PB) and PB cyanometalate structural analogues (PBAs), composed of Fe^{3+}, Fe^{2+} or other metal ions and bridging cyano groups, are representative coordinative polymers with three-dimensional (3D) networks [25–27]. PB and PBAs typically possess a face-centered cubic crystal structure with $Fm\bar{3}m$ space group, in which the transition metal ions are linked together through cyanide ligands [28]. It has been reported that PB and PBAs with special composition and structure possess peroxidase-like activity. Inspired by the biomimetic mineralization and facile synthesis conditions of PB and PBAs, which are compatible with biomolecules, we anticipate that the intrinsically stable structure of the PBAs may endow a natural enzyme with enhanced stability upon its successful combination with the inorganic host. However, artificial multienzyme systems containing PBAs and natural enzymes constructed via biomimetic mineralization have not yet been investigated. These systems would further expand the scope of PBAs and natural enzymes in biocatalysis or biosensing. Thus, this study aimed to explore the feasibility of constructing a hybrid multienzyme system and its potential applications.

The detection of the glucose concentration is vital in many fields, such as medical diagnosis, food quality control, and fermentation [19, 29]. The diagnosis and monitoring of diabetes rely on the detection of glucose levels in blood and urine. Thus, the development of a sensitive glucose sensor is essential for practical applications. The conventional detection of glucose involves two separate steps: glucose is first oxidized to generate hydrogen peroxide, which then reacts with a chromogenic substrate under peroxidase catalysis to generate detectable signals. However, the instability of hydrogen peroxide and its diffusion as intermediate into the bulk solution leads to a low sensitivity of this assay.

In this study, a copper analogue of Prussian blue (CPB) with peroxidase-mimic activity was chosen as a supporting matrix for the in situ encapsulation of glucose oxidase (GOx), to construct an artificial multienzyme system (denoted as GOx@CPB, @ denotes the encapsulation of GOx in CPB) via biomimetic mineralization. This CPB-mediated multienzyme system was capable of catalyzing the cascade reaction of glucose oxidation and generating detectable signals in a one-pot reaction with high efficiency, which enables the detection of low glucose concentrations. Moreover, the GOx@CPB system exhibited enhanced storage stability and reusability compared to the free enzyme. The encapsulated GOx exhibited improved stability under unfavorable conditions such as organic solvents or denaturing and proteolytic agents, which resulted from the protection of the external CPB shell. This strategy enables the successful construction of an artificial multienzyme system composed of natural enzymes and enzyme mimics, and provides new opportunities for the investigation of cooperative effects of chemo-catalysts and natural biocatalysts.

2 Materials and Methods

2.1 Materials

Potassium ferricyanide ($K_3[Fe(CN)_6]$), ferrous chloride ($FeCl_2$), cupric chloride dihydrate ($CuCl_2{\cdot}2H_2O$),

dimethylsulfoxide (DMSO), sodium dodecyl sulfate (SDS), glucose, fructose, galactose, arabinose, mannose, xylose, sucrose, sucrose and hydrogen peroxide (30 wt%) were purchased from Guangzhou chemical reagent factory. 3, 3′, 5, 5′-tetramethylbenzidine (TMB) and 2,2′-Azino-bis (3-ethylbenzothiazoline-6-sulfonic acid) diammonium salt (ABTS) were purchased from Sigma-Aldrich. Glucose oxidase (GOx), horseradish peroxidase (HRP) and papain were obtained from Sangon Biotech (Shanghai) Co., Ltd. All of the reagents were used as received.

2.2 Preparation of CPB and GOx@CPB

CPB was prepared through the following method. In a typical reaction system, 2.5 mL of aqueous solution containing 5 mM of $FeCl_2$ and 2.5 mM of $CuCl_2$ was incubated at 60 °C for 5 min and then cooled down to room temperature (25 °C). 2.5 mL of $K_3[Fe(CN)_6]$ solution (5 mM) was added into the above solution under stirring (200 rpm) and reacted at room temperature for 5 min. The obtained material was separated by centrifugation (12,000 rpm, 1 min) and then washed with DI water for 3 times. The synthesis of GOx encapsulated inside CPB (GOx@CPB composite) followed the similar procedure, except for GOx (0.5 mg) was added to the cooled down solution of $FeCl_2$ and $CuCl_2$. Following the same preparation and washing process, sample of GOx@CPB composite was prepared.

2.3 Enzymatic Activity Assay of GOx, CPB and GOx@CPB Composite

The enzymatic activity of GOx was detected by measuring the oxidation reaction rate of glucose. In a typical reaction, 50 µL of GOx aqueous solution (0.05 mg/mL) or equivalent immobilized GOx was quickly mixed with 950 µL of acetate buffer (pH 4.5, 50 mM) containing 100 mM of glucose, 5 mM of ABTS and 0.05 mg/mL of HRP to initiate the reaction. The increase of absorbance at 415 nm within 1 min was recorded by the UV–Vis spectrophotometer (Shimadzu, UV-2550) and the initial activity was defined as enzymatic activity. Meanwhile, the mimetic peroxidase activity of CPB was determined by measuring the decomposition rate of hydrogen peroxide with ABTS as the hydrogen donor. In this case, 50 µL of CPB dispersion was added into 950 µL acetate buffer containing H_2O_2 (10 mM) and ABTS (5 mM) to start the reaction. The increase of absorbance of the reaction solution at 415 nm was monitored immediately after catalyst was added. The experiment was done independently in triplicate. The error bars in this study were obtained by calculating the standard deviation of results of parallel experiments.

The activity of GOx@CPB composite was measured as follows. GOx@CPB composite dispersion (50 µL) was added into 950 µL of acetate buffer containing 100 mM of glucose and 5 mM of ABTS to catalyze the cascade reaction. The increase of absorbance at 415 nm was measured and the reaction rate was calculated. Moreover, by fitting of Michaelis–Menten equation, the catalytic constants such as K_m, V_{max} were calculated. Michaelis–Menten equation is as follows.

$$V_0 = V_{max}\frac{[S]}{K_m + [s]}$$

V_0 stands for the initial reaction velocity and V_{max} represents the maximal reaction velocity. [S] stands for the substrate concentration.

2.4 Limit of Detection of GOx@CPB Composite

The limit of detection of GOx@CPB composite was investigated as following: 50 µL of GOx@CPB composite (0.05 mg/mL) solution was added to 950 µL of acetate buffer containing TMB (1.2 mM) and gradient concentration of glucose (0.5, 1, 5, 10, 15, 20, 40, 60, 80, 100 µM) to start the reaction, the variation of absorbance at 635 nm in 60 min was determined.

2.5 Substrate Selectivity of GOx@CPB Composite

To investigate the specificity of glucose detection with GOx@CPB, fructose, galactose, arabinose, xylose, mannose, maltose and sucrose were applied as substrates for the catalytic process. 50 µL of GOx@CPB composite suspension (0.05 mg/mL) was added to 950 µL of acetate buffer containing TMB (1.2 mM) and the aforementioned saccharides (3 mM), with concentration were ten times of glucose under identical detection. The increased absorbance at 635 nm after 60 min reaction was measured on a UV/Vis spectrophotometer. The experiment was done independently in triplicate.

3 Results and Discussion

3.1 Characterization of CPB and GOx@CPB

As shown in Scheme 1, in a typical experiment, an aqueous solution of $K_3[Fe(CN)_6]$ was added into a solution containing $FeCl_2$ and $CuCl_2$, followed by gentle stirring for 5 min. The obtained precipitate was denoted as CPB. PB has a cubic structure with Fe^{2+} and Fe^{3+} cations on alternate corners of a cubic lattice of corner-sharing octahedra bridged by linear C≡N anions [27]. In the structure of CPB, part of the Fe^{2+} and Fe^{3+} cations are replaced by Cu^{2+} ions, bridged by linear C≡N units. The preparation of the GOx@CPB

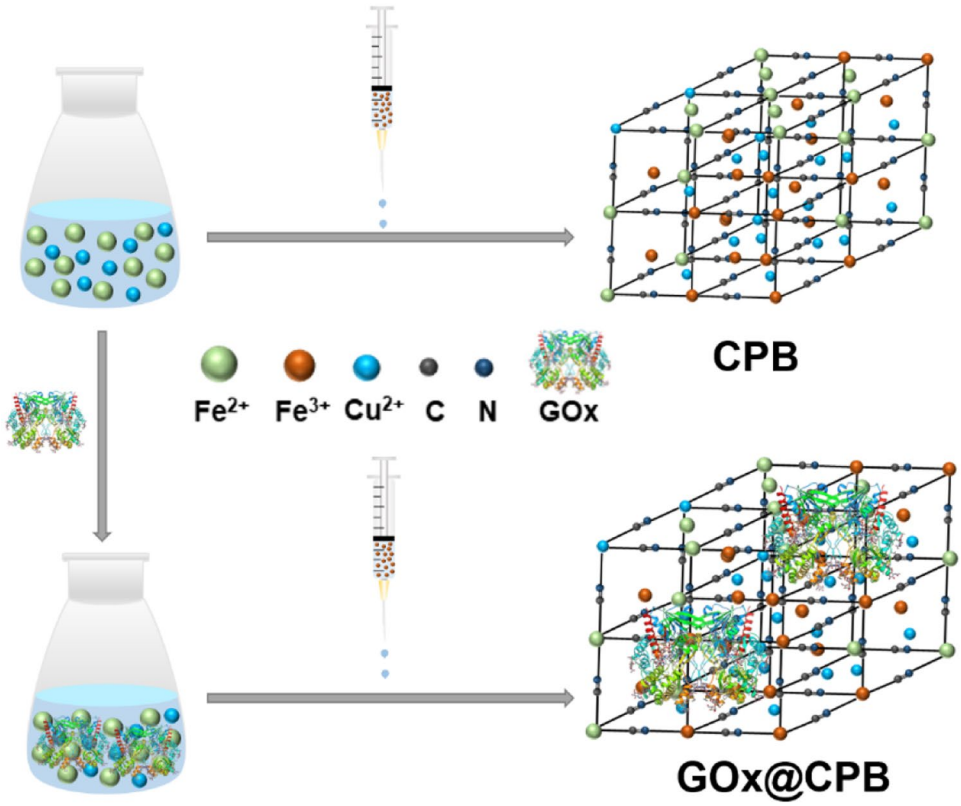

Scheme 1 Schematic illustration of the preparation of CPB and GOx@CPB

composite followed a similar procedure, with the further addition of GOx into the $FeCl_2$/$CuCl_2$ solution.

Scanning electron microscopy (SEM) measurements were carried out to inspect the morphology of CPB and GOx@CPB. The SEM image in Fig. 1a shows that CPB exhibited an irregular round shape and an average particle diameter of 10 nm. After the introduction of GOx, the morphology of the composite changed into a regular circular shape with a particle diameter of approximately 20 nm (Fig. 1b). This increase in particle size may be attributed to the accumulation of metal ions by GOx during the biomimetic mineralization process. Moreover, as revealed by the energy-dispersive X-ray spectroscopy (EDS) mappings in Fig. 1c, the distribution of C, N, Fe, and Cu in CPB particles was uniform, confirming the successful incorporation of Cu into the framework of PB.

The ultraviolet–visible (UV–Vis) spectrum of the obtained CPB showed a shift in the peak at ~ 740 nm compared to the absorption peak of conventional Prussian blue at 700 nm [30], which resulted from the introduction of Cu^{2+} (Fig. 2a). After incorporation of GOx, this peak further shifted to 745 nm, reflecting the interaction between GOx and CPB during the biomimetic mineralization process. To further characterize the chemical group composition of CPB and GOx@CPB, Fourier transform infrared (FTIR) spectroscopy measurements were carried out (Fig. 2b). The absorption band located at 2070 cm^{-1} could be attributed to the C≡N stretching vibration of CPB and GOx@CPB. The peaks at 433 and 593 cm^{-1} resulted from the adsorption of Cu–C≡N and Fe–C≡N, respectively. After the introduction of GOx, we observed bands at 1540 and 1640 cm^{-1} assigned to amide II and amide I bonds, respectively, indicating the successful incorporation of GOx in the composite. The loading amount of GOx in the GOx@CPB composite was determined by thermogravimetric analysis (TGA) (Fig. 2c). The 20% weight loss between 30 and 100 °C was ascribed to the evaporation of water. In the temperature range from 130 to 300 °C, CPB exhibited a 24.6% weight loss, corresponding to its decomposition. On the other hand, an obvious weight loss of 30.3% was observed for the GOx@CPB composite. The apparent higher decomposition percentage indicated the decomposition of GOx within this range, calculated to be 5.7 wt%. The encapsulation of GOx was quantified by measuring the protein amount left in the supernatant immediately after the synthesis, which indicated an immobilization efficiency of 100%. X-ray diffraction (XRD) patterns were obtained to examine the crystal structure of CPB and its change after incorporating GOx. The GOx@CPB composite exhibited peaks consistent with those of CPB (Fig. 2d), suggesting that the incorporation of GOx did not alter the crystallinity of CPB.

X-ray photoelectron spectroscopy (XPS) measurements were carried out to further investigate the chemical composition and electronic states of CPB and GOx@CPB

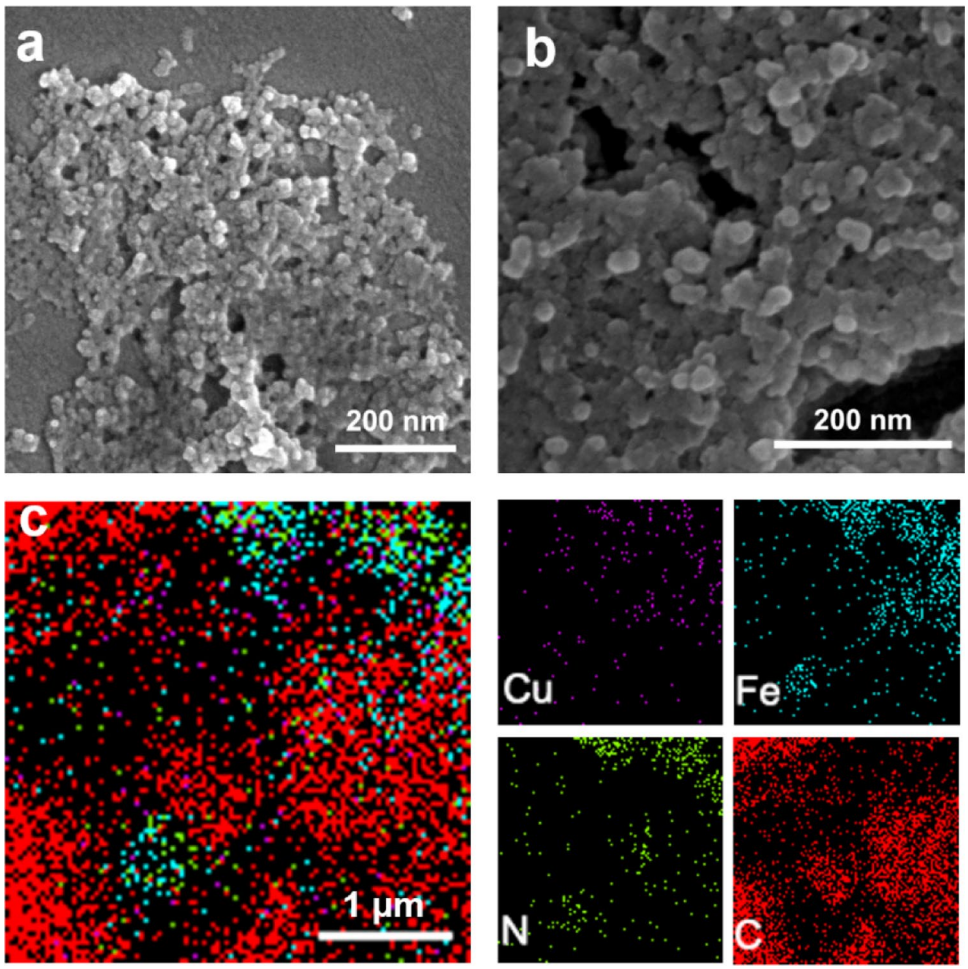

Fig. 1 Microscopic morphology and elemental distribution of CPB and GOx@CPB. **a** and **b** SEM images of CPB (**a**) and GOx@CPB composite (**b**). **c** EDS mappings of Cu, Fe, N, and C elemental distributions in CPB

(Fig. 3). The full spectra revealed the presence of C, N, Cu, Fe, and O (Fig. 3a). The distinct and symmetrical peak at 397.4 eV in the high-resolution N 1 s spectrum (Fig. 3b) reflects the unique chemical environment of N in CPB, which was attributed to the C≡N interaction. The peak at 397.6 eV, corresponding to the C≡N group, was still present after incorporation of GOx. The new peak at 399.1 eV was ascribed to the amide group in GOx, suggesting the successful encapsulation of GOx in the GOx@CPB composite. The high-resolution Cu $2p_{3/2}$ spectrum (Fig. 3c) displays peaks at 932.8 and 935.6 eV, corresponding to the Cu^{+} and Cu^{2+} oxidation states. Based on the calculated peak areas, Cu^{+} accounted for a small portion of the copper content in the composite. The appearance of Cu^{+} in CPB implies that some of the copper ions were reduced during the formation of CPB. The spectrum of the GOx@CPB composite sample shows four peaks at 932.7, 952.5, 935.5, and 955.4 eV, which were assigned to Cu^{+} $2p_{3/2}$, Cu^{+} $2p_{1/2}$, Cu^{2+} $2p_{3/2}$, and Cu^{2+} $2p_{1/2}$, respectively. The shift in binding energy reflects the interaction between Cu^{+}/Cu^{2+} and GOx during the biomimetic mineralization process. The Fe 2p XPS spectra of CPB show peaks at 708.6, 721.5, 711.7, and 724.5 eV, attributed to Fe^{2+} $2p_{3/2}$, Fe^{2+} $2p_{1/2}$, Fe^{3+} $2p_{3/2}$, and Fe^{3+} $2p_{1/2}$, respectively (Fig. 3d). After the introduction of GOx, these binding energies slightly shifted to 708.5, 721.4, 711.6, and 724.4 eV, respectively. Compared with Prussian blue, the contents of Fe^{2+} in CPB and GOx@CPB were higher than those of Fe^{3+}, which may be attributed to the competitive binding between Fe^{3+} and Cu^{2+} with Fe^{2+}.

3.2 Catalytic Performance of GOx@CPB

The catalytic activity of CPB was then investigated. As expected, CPB exhibited peroxidase-like activity. Using 2,2′-Azino-bis (3-ethylbenzothiazoline-6-sulfonic acid) diammonium salt (ABTS) as the chromogenic agent and hydrogen peroxide (H_2O_2) as substrate, CPB initiated the reaction immediately, and the reaction solution turned green. The control experiment showed that, in the absence of CPB, the reaction system containing H_2O_2 and ABTS only exhibited a slight increase in absorbance at 415 nm. Furthermore, the catalytic activity of CPB was evaluated with glucose as substrate, and the results showed that CPB had no GOx-like catalytic activity. Upon changing the initial enzyme

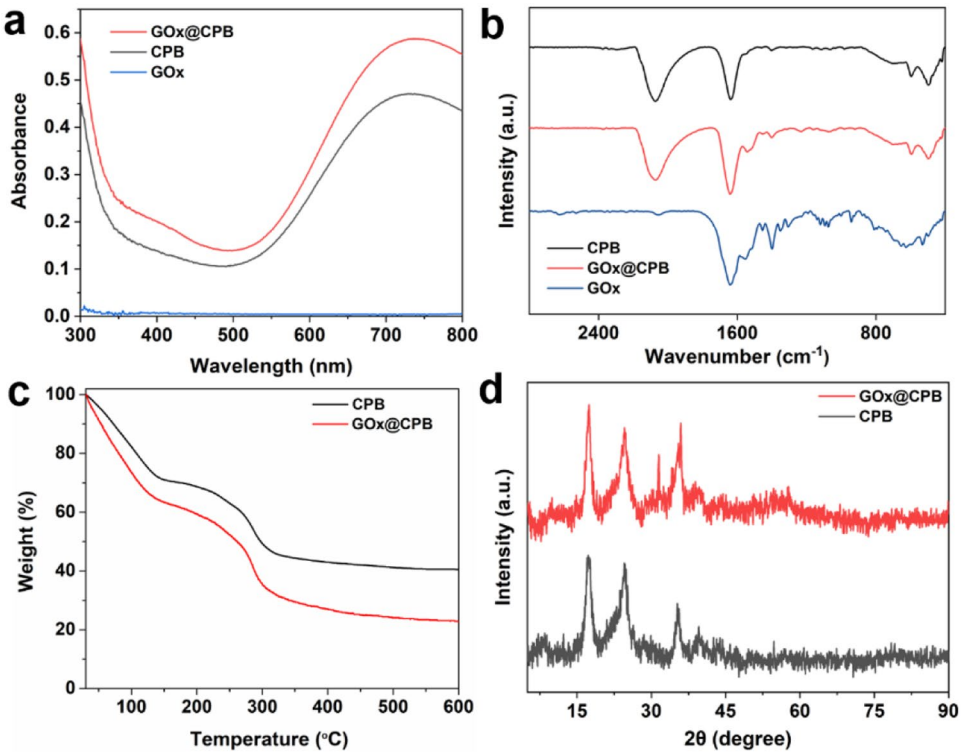

Fig. 2 Characterization of CPB and GOx@CPB. UV–Vis (**a**) and FTIR (**b**) spectra of GOx, CPB, and GOx@CPB composite. TGA curves (**c**) and XRD patterns (**d**) of CPB and GOx@CPB composite

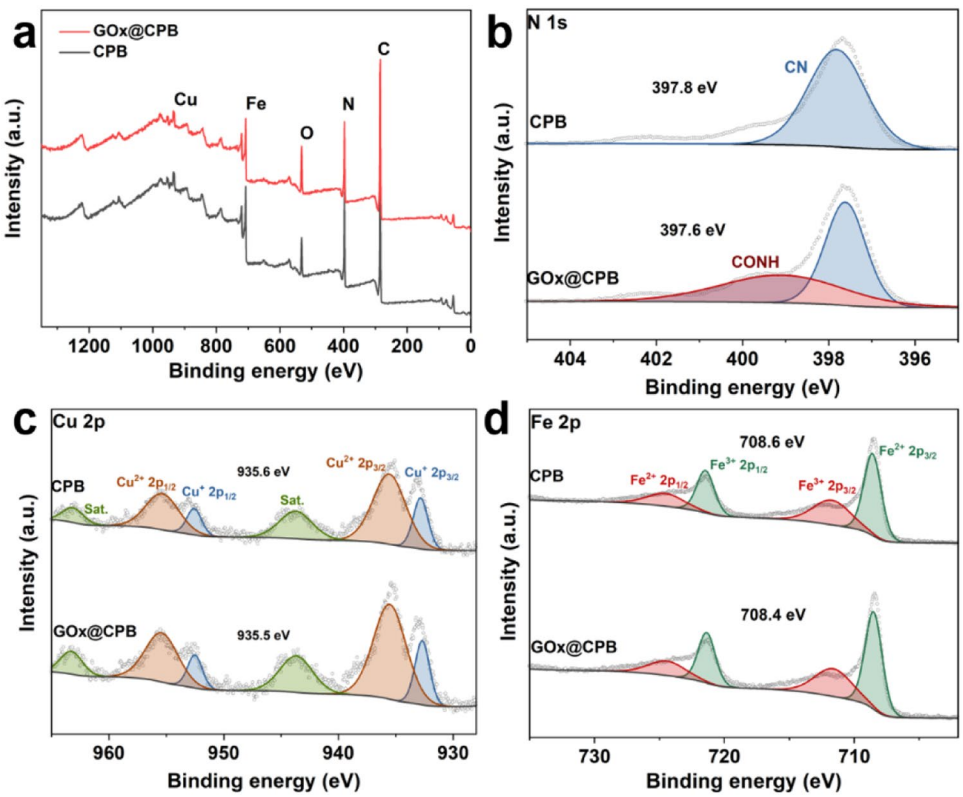

Fig. 3 XPS profiles of CPB and GOx@CPB. Full spectra (**a**) and high-resolution N (**b**), Cu (**c**), and Fe (**d**) profiles

concentration during the preparation, the obtained GOx@CPB composite did not show changes in activity compared with CPB. This phenomenon indicates that the incorporation of GOx did not lead to obvious structural changes in CPB, which might affect the number of catalytic sites and thus lead to changes in its activity. By defining 1 unit (U) of GOx as the amount of enzyme required to catalyze glucose oxidation and generate 1 μmol hydrogen peroxide within 1 min, the enzyme activities of free GOx and GOx@CPB are 573 U and 410 U respectively.

Based on the above analysis, the cascade reaction initiated by GOx@CPB was carried out in a one-pot process. Glucose was first oxidized by GOx with oxygen to generate gluconic acid and H_2O_2 [17]. Then, colorless 3, 3′, 5, 5′-tetramethylbenzidine (TMB) was oxidized by H_2O_2 to generate blue TMB^+ [31] under the catalysis of CPB (Fig. 4a). In this study, the GOx@CPB composite was added to an acetate buffer containing TMB and different concentrations of glucose, and the absorbance at 635 nm was determined in 60 min. As the glucose concentration ranged from 0.5 to 100 μM, the color of the supernatant changed from light to dark blue, and the change could be observed by the naked eye (Fig. 4b, inset). The absorbance at 635 nm showed a good linear relationship, with $R^2 = 0.9997$ within the detected range of glucose concentrations. The limit of detection (LOD) was calculated to be 0.48 μM, which is lower than that of most reported glucose detection methods [32–35]. This outstanding catalytic performance possibly originated from the accumulation of intermediates, which were immediately utilized by the GOx@CPB composite due to proximity effects. Therefore, the highly efficient utilization of intermediates led to the enhanced catalytic performance of the GOx@CPB composite and a higher sensitivity in the detection of glucose.

In addition, we investigated the selectivity of GOx toward different substrates after incorporation in CPB. We carried out experiments with substrates including fructose, galactose, mannose, arabinose, xylose, maltose, and sucrose in concentrations ten times that of glucose, containing equivalent amounts of GOx@CPB composite as catalyst. As shown in Fig. 4c, the absorbances at 635 nm obtained with the other substrates were considerably lower than that of the glucose solution, which could be distinguished by the naked eye (Fig. 4c, inset). This confirmed the high specificity toward glucose of the present colorimetric assay based on the GOx@CPB composite.

To evaluate the catalytic activity of GOx and GOx@CPB with glucose as substrate, the kinetic parameters were measured by fitting the experimental data with the Michaelis–Menten equation (Fig. 5a). Free GOx exhibited a K_m value of 30.8 mM, while GOx@CPB showed a slightly lower K_m of 28.6 mM, suggesting that GOx incorporated inside CPB exhibited higher affinity towards glucose, which can be ascribed to the adsorption and accumulation of substrates over the supporting scaffold [36]. Moreover, the GOx@CPB composite showed k_{cat} and k_{cat}/K_m values of 4.1 s^{-1} and

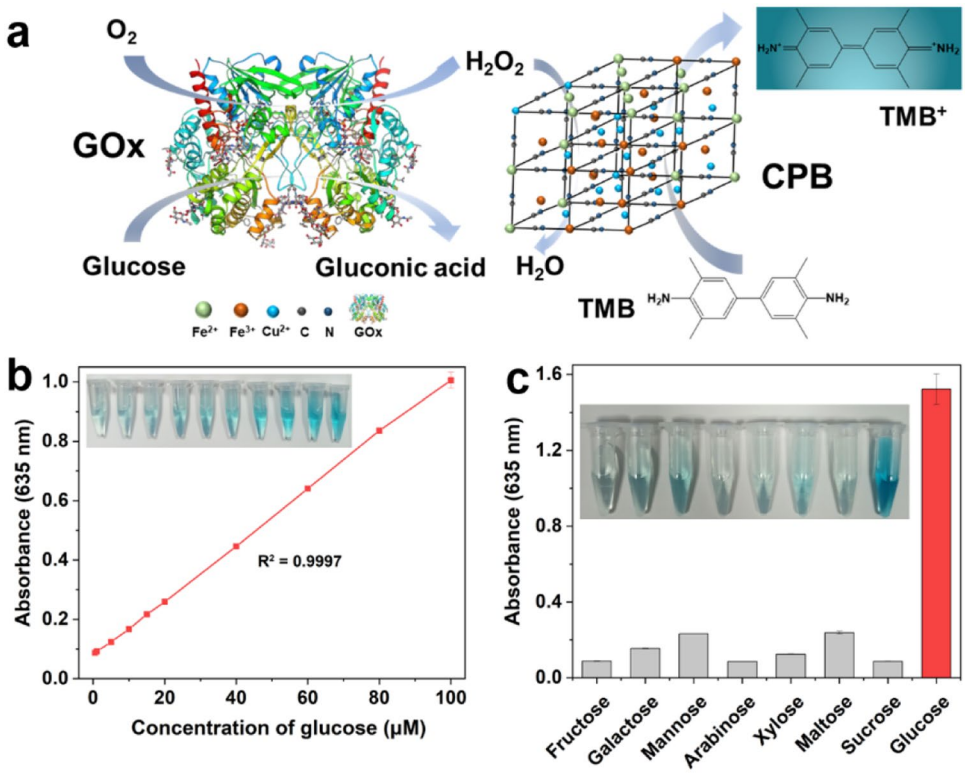

Fig. 4 Detection of glucose with GOx@CPB. **a** Cascade reaction based on GOx@CPB composite. **b** Absorbance of glucose concentrations ranging from 0.5 to 100 μM, under catalysis by GOx@CPB composite. Inset: photograph showing color changes of the supernatant with increasing glucose concentration (0.5–100 μM; from left to right, the concentration was 0.5, 1, 5, 10, 15, 20, 40, 60, 80, and 100 μM). **c** Selectivity of GOx@CPB composite toward saccharides. Inset: photograph showing the color of each reacted solution. From left to right: solutions containing 3.0 mM fructose, galactose, mannose, arabinose, xylose, maltose and sucrose, along with 300 μM glucose

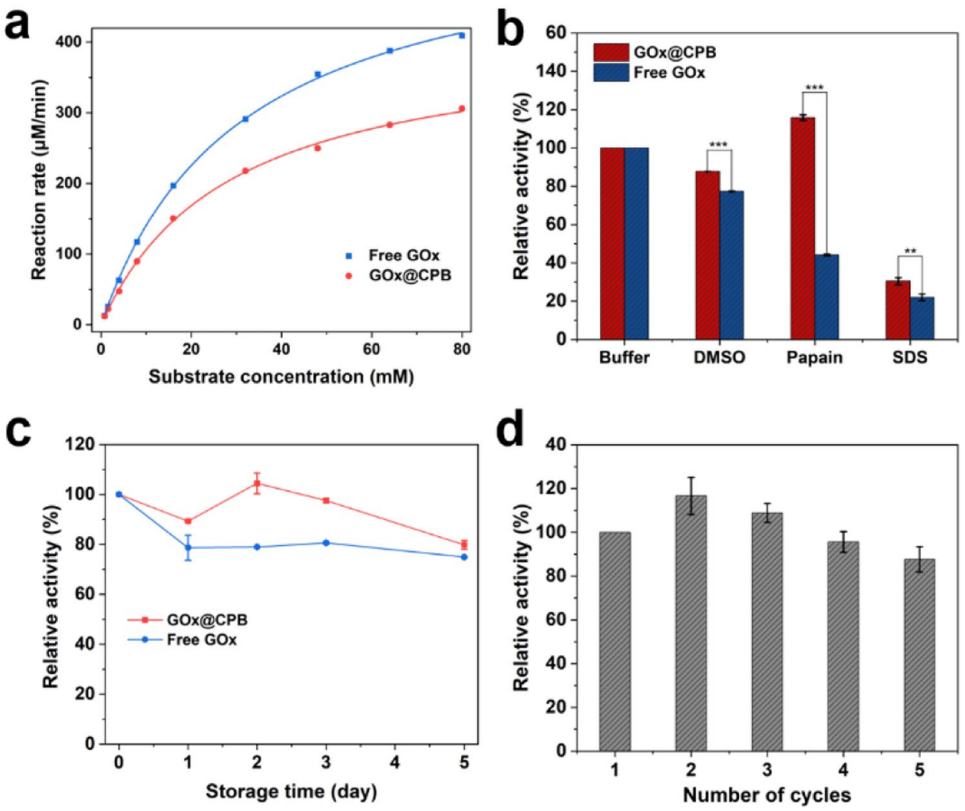

Fig. 5 Enzyme activity and stability of GOx@CPB. **a** Michaelis–Menten fitting of GOx and GOx@CPB composite. **b** Relative activities of GOx and GOx@CPB composite after incubation in DMSO, papain, and SDS for 60 min. ns: $P > 0.05$; *$P < 0.05$; **$P < 0.01$; ***$P < 0.001$. **c** Long-term storage stability of GOx and GOx@CPB composite over 5 days. **d** Recycling performance of GOx@CPB composite over five cycles. Each experiment was repeated independently three times

0.14 s^{-1}·mM^{-1}, respectively, while the corresponding values for free GOx were 5.7 s^{-1} and 0.19 s^{-1}·mM^{-1}, respectively. These results demonstrated that GOx@CPB composite prepared via biomimetic mineralization exhibited comparable catalytic performance compared to free GOx.

The stability of enzyme under unfavorable conditions is an important parameter for practical applications, such as those involving organic solvents, denaturing and proteolytic agents. The stability of the present system was assessed by comparing the activity of the free and encapsulated enzymes upon exposure to identical treatment conditions for the same time. DMSO is an excellent solvent for dissolving substrates with high molecular weight during catalysis. However, it tends to strip essential water molecules from the surface of enzymes, leading to unfavorable conformational changes and loss of the catalytic function of the enzyme. Genetic engineering is an effective method to enable the enzyme to function in DMSO-containing solutions. The encapsulation of the enzyme provides another route to enhance its tolerance to DMSO solutions. Thus, we evaluated the stability of the enzyme in DMSO. As shown in Fig. 5b, after incubation in DMSO (99%, v/v) for 60 min at 37 °C, GOx@CPB retained 85% of its initial activity, whereas only 75% of the original activity was detected for free GOx. This result indicates that PB inhibited the attack from the organic solvent to the encapsulated enzyme. Proteolytic enzymes hydrolyze proteins and peptides, which are widely found in plants and animals. Therefore, we also evaluated the stability of GOx@CPB against the proteolytic enzyme papain. In this case, the GOx@CPB composite maintained almost 110% of its initial activity, whereas only 40% of the initial activity of free GOx was retained. The activity of the enzyme in the presence of the SDS denaturing agent was also assessed. The activity retention of the GOx@CPB composite in the presence of SDS was 10% higher than that of free GOx. The excellent catalytic performance of the GOx@CPB composite in harsh environments can be attributed to the shielding effect of the CPB shell. Thus, we demonstrated that the CPB shell could provide a protecting function for the encapsulated enzyme, without affecting its activity. The long-term storage stability of the GOx@CPB composite was also assessed by incubating GOx and GOx@CPB in acetate buffer for 5 days. On each individual day, the activity retention of GOx@CPB was higher than that of free GOx. After storage for 5 days, GOx@CPB exhibited an almost identical activity retention to the free enzyme (Fig. 5c). Moreover, the GOx@CPB composite could be recycled five times without obvious activity loss (Fig. 5d). The slight activity decrease can be attributed to the loss of nanosized particle during the centrifugation process for reuse. In terms of specific activity, the activity of GOx@CPB composite was fully retained. Therefore, GOx@CPB composite exhibited good operational stability, showing great potential in practical application.

4 Conclusion

A multienzyme system was successfully constructed via biomimetic mineralization, with CPB acting as peroxidase inorganic mimic and encapsulating the natural enzyme, GOx. The incorporation of GOx did not lead to obvious structural changes in CPB. The developed GOx@CPB composite drove the cascade reaction in which glucose was oxidized by GOx yielding hydrogen peroxide as intermediate, which was subsequently catalyzed by the surrounding CPB to generate a detectable signal. Thus, the GOx@CPB composite functioned as a colorimetric biosensor for the detection of glucose at low concentrations. Moreover, the CPB shell provided an ideal protection to the encapsulated GOx when exposed to unfavorable environments, including organic solvents and denaturing or proteolytic agents. Therefore, the present facile strategy for the construction of hybrid multienzyme systems shows a promising potential for the development of biosensors and biocatalysts.

Supplementary Information The online version contains supplementary material available at https://doi.org/10.1007/s10562-021-03668-8.

Acknowledgements We gratefully acknowledge the National Natural Science Foundation of China (21908070, 21878105), Introduced Innovative R&D Team Leadership of Dongguan City (2020607263005), China Postdoctoral Science Foundation (BX20180102, 2019M652902), Science and Technology Program of Guangzhou (201904010360, 202002030398), and the Fundamental Research Funds for the Central Universities (2019MS100, 2019PY15) for financial support.

Author Contributions XLW and WYL conceived the idea and designed the experiments. BC performed the experiments. XLW, BC and WYL analyzed the results. JX, MHZ, JHC and JG participated in the analysis of the data. XLW and BC wrote the paper. WYL supervised the project.

Data Availability All data generated or analysed during this study are included in this published article.

Declarations

Conflict of interest The authors declare no conflict of interest.

References

1. Liu M, He S, Cheng L, Qu J, Xia J (2020) Biomacromol 21:2391–2399
2. Sperl JM, Sieber V (2018) ACS Catals 8:2385–2396
3. Rezaei S, Landarani-Isfahani A, Moghadam M, Tangestaninejad S, Mirkhani V, Mohammadpoor-Baltork I (2019) Chem Eng J 356:423–435
4. Sheldon RA, van Pelt S (2013) Chem Soc Rev 42:6223–6235
5. Sakdaphetsiri K, Thaweeskulchai T, Schulte A (2020) Chem Commun 56:7132–7135
6. Bornsuer UT, Hauer B, Jaeger KE, Schwaneberg U (2019) Angew Chem Int Edit 58:36–40
7. Fleming SR, Bartges TE, Vinogradov AA, Kirkpatrick CL, Goto Y, Suga H et al (2019) J Am Chem Soc 141:758–762
8. Wang A, Sudarsanam P, Xu Y, Zhang H, Li H, Yang S (2020) Green Chem 22:2977–3012
9. Müller J, Niemeyer CM (2008) Biochem Biophys Res Commun 377:62–67
10. Liu F, Banta S, Chen W (2013) Chem Commun 49:3766–3768
11. Monteiro RRC, Santos JCSD, Alcántara AR, Fernandez-Lafuente R (2020) Catalysts 10:891
12. Okura NS, Sabi GJ, Crivellenti MC, Gomes RAB, Mendes AA (2020) Int J Biol Macromol 163:550–561
13. Jiang B, Yan L, Zhang J, Zhou M, Shi G, Tian X et al (2019) ACS Appl Mater Interfaces 11:9747–9755
14. Wang Z, Zhang Y, Ju E, Liu Z, Cao F, Chen Z et al (2018) Nat Commun 9:3334
15. Sang Y, Cao F, Li W, Zhang L, You Y, Deng Q et al (2020) J Am Chem Soc 42:5177–5183
16. Kang L, Ricco R, Doherty CM, Styles MJ, Bell S, Kirby N et al (2015) Nat Commun 6:7240
17. Chen W, Margarita VG, Amani Z, Raed AR, Itamar W (2018) Nat Catal 1:689–695
18. An H, Li M, Gao J, Zhang Z, Ma S, Chen Y (2019) Coord Chem Rev 384:90–106
19. Wu X, Yue H, Zhang Y, Gao X, Li X, Wang L et al (2019) Nat Commun 10:5165
20. Chen S, Lo W, Huang Y, Si X, Liao F, Lin S et al (2020) Nano Lett 20:6630–6635
21. Liang S, Wu X, Xiong J, Zong M, Lou W (2020) Coord Chem Rev 406:213149
22. Feng Y, Wang H, Zhang S, Zhao Y, Gao J, Zheng Y et al (2019) Adv Mater 31:1805148
23. He C, Lu K, Liu D, Lin W (2014) J Am Chem Soc 136:5181–5184
24. Kang L, Richardson JJ, Cui J, Caruso F, Doonan CJ, Falcaro P (2016) Adv Mater 28:7910–7914
25. Buser HJ, Schwarzenbach D, Petter W, Ludi A (1977) Inorg Chem 16:2704–2710
26. Marquez C, Cirujano FG, Van Goethem C, Vankelecom I, De Vos D, De Baerdemaeker T (2018) Catal Sci Technol 8:2061–2065
27. Vázquez-González M, Torrente-Rodríguez RM, Kozell A, Liao WC, Cecconello A, Campuzano S et al (2017) Nano Lett 17:4958–4963
28. Wang W, Feng J, Ye Y, Lyu F, Yin Y (2017) Nano Lett 17:755–761
29. Kalaivani GJ, Suja SK (2019) Food Chem 298:124981
30. Wu X, Xiong J, Liu S, Chen B, Liang S, Lou W et al (2020) ChemCatChem 12:1996–1999
31. Zhang P, Sun D, Cho A, Weon S, Choi W (2019) Nat Commun 10:940
32. Hou C, Wang Y, Ding Q, Jiang L, Li M, Zhu W et al (2015) Nanoscale 7:18770–18779
33. Wang Q, Zhang X, Huang L, Zhang Z, Dong S (2017) Angew Chem Int Edit 129:16298–16301
34. Wu X, Ge J, Yang C, Hou M, Liu Z (2015) Chem Commun 51:13408–13411
35. Madhusudhan A, Park SC, Bandi R, Lee SH, Kim JC (2020) Carbohyd Polym 253:117239
36. Cheng KP, Svec F, Lv YQ, Tan TW (2019) Samll 44:1902927

Authors and Affiliations

Bin Chen[1] · Xiaoling Wu[1] · Jun Xiong[1] · Min-Hua Zong[1] · Jian-Hua Cheng[2] · Jun Ge[3] · Wen-Yong Lou[1,2]

✉ Xiaoling Wu
wuxl18@scut.edu.cn

✉ Wen-Yong Lou
wylou@scut.edu.cn

[1] Lab of Applied Biocatalysis, School of Food Science and Engineering South, China University of Technology, No. 381 Wushan Road, Guangzhou 510640, Guangdong, China

[2] South China Institute of Collaborative Innovation, Xuefu Road, Dongguan 523808, Guangdong, China

[3] Key Lab for Industrial Biocatalysis, Ministry of Education, Department of Chemical Engineering, Tsinghua University, Beijing 100084, China